Supplementary information for:

Metal sensing and signal transduction by CnrX from *Cupriavidus metallidurans* CH34: role of the only methionine assessed by a functional, spectroscopic, and theoretical study.

Juliette Trepreau, Cornelia Grosse, Jean-Marie Mouesca, Géraldine Sarret, Eric Girard, Isabelle Petit-Haertlein, Sandra Kuennemann, Céline Desbourdes, Eve de Rosny, Antoine P. Maillard, Dietrich H. Nies, and Jacques Covès

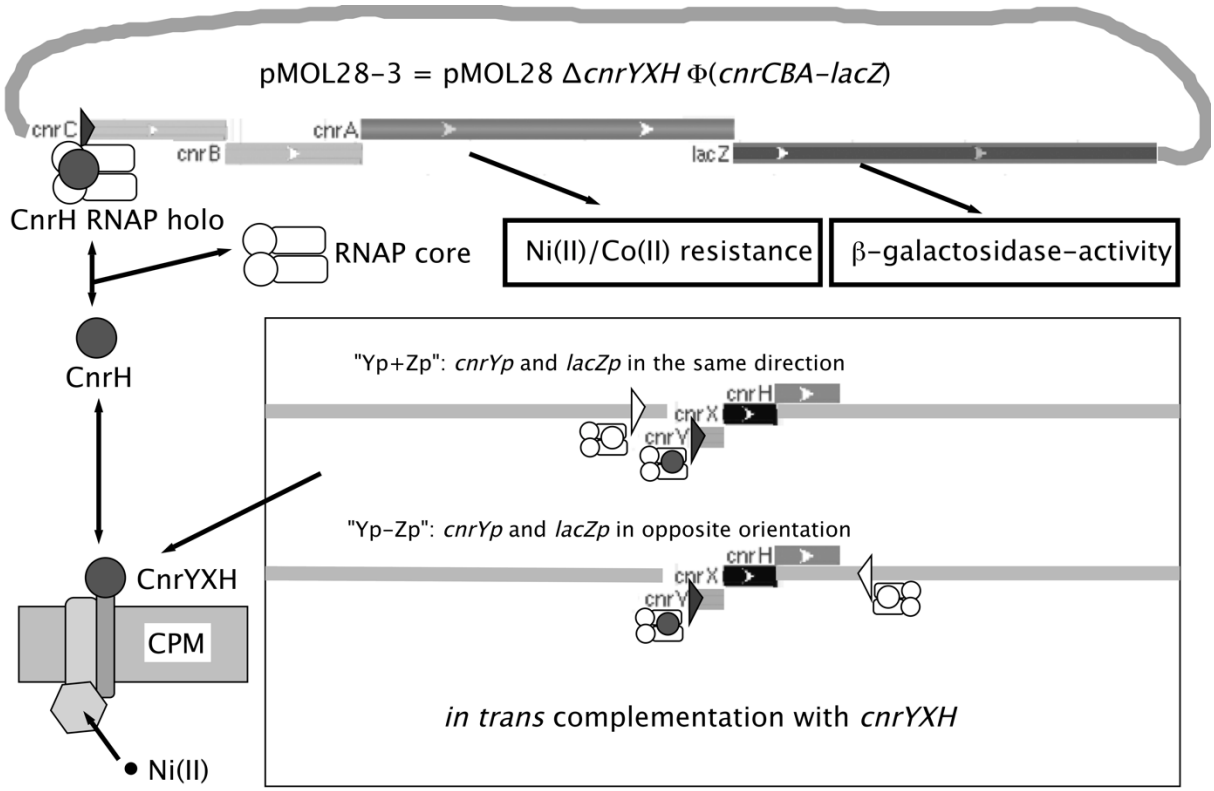

Fig. SI1. Experimental set-up for *in vivo* experiments. The *cnrX* gene was mutated and cloned as part of the *cnrYXH* operon in plasmid pBBR1, either in the same direction as the *lacZp* promoter on this vector plasmid ("Yp + Zp") or in the opposite orientation ("Yp – Zp"). In both cases, the *cnrYXH* region is expressed under control of the *cnrYp* promoter. The *lacZp* promoter is constitutive in *C. metallidurans*. The plasmids were transferred into a *C. metallidurans* strain DN190 that contains plasmid pMOL28-3 Δ*cnrYXH* Φ(*cnrCBA-lacZ)*. Since promoters (black arrow heads) *cnrCp* and *cnrYp* depend on the CnrH-RNA polymerase holoenzyme, it is necessary to obtain metal resistance and β-galactosidase activity that (i) a CnrYXH complex is inserted into the cytoplasmic membrane (CPM), (ii) CnrH is being released, e.g. after binding of nickel to CnrX, (iii) the CnrH-RNAP-holoenzyme is being formed, (iv) leading to expression of *cnrCBA-lacZ* from plasmid pMOL28-3 and *cnrYXH* from the vector plasmid *in trans*. The *lacZp* promoter (open arrow head) on this vector depends on the house keeping RpoD-RNAP holoenzyme, so that expression of *cnrYXH* is also possible if CnrH is not being produced or released. A gray filled circle at the RNA polymerase holoenzyme indicates CnrX while an open circle RpoD.

Table SI1: Data collection and refinement statistics

	Native
Data collection	
Space group	$P2_1$
Cell dimensions	
a, *b*, *c* (Å)	31.85, 79.12, 93.47
β (°)	90.10
Wavelength (Å)	0.8726
Resolution (Å)	46.74-1.85 (1.95-1.85)
R_{merge}	0.086 (0.968)
R_{pim}	0.065 (0.726)
*CC1/2**	0.998 (0.598)
$I / \sigma(I)$	11.3 (1.5)
Completeness (%)	99.5 (98.0)
Redundancy	5.3 (5.3)
Refinement	
Resolution (Å)	46.74-1.85
No. reflections	39447
R_{work} / R_{free}	0.176 / 0.222
No. atoms	
Protein	3594
Ni	4
Water	186
Ligands	64
Mean *B*-factors (Å^2)	
Protein	32.20
Water	42.20
R.m.s deviations	
Bond lengths (Å)	0.005
Bond angles (°)	0.88
Ramachandran	
Favored (%)	98.0
Outliers (%)	0.68

Diffraction data were integrated with XDS (5) and integrated intensities were scaled and merged using AIMLESS and TRUNCATE from the CCP4 suite of programs (6).
*CC1/2 = percentage of correlation between intensities from random half-datasets (7).

5. Kabsch, W. (2010) XDS. *Acta Cryst.* **D66**, 125-132.
6. Collaborative Computational Project, Number 4 (1994) *Acta Crystallogr. Sect. D.* **50**, 760-763.
7. Karplus, P. A., and Diederichs, K. (2012) Linking crystallographic data with model quality. *Science* **336**, 1030-1033.

Table SI2. Ni to ligand atom distances (Å)

	CnrXs	M123A-CnrXs
Equatorial ligands		
Nε2 His42	2.10	2.04
Nε2 His46	2.12	2.20
Nε2 His119	2.16	2.12
O2 Glu63	2.20	1.92
Axial ligands		
O1 Glu63	2.23	2.28
Sδ Met123	2.45	-----
Water	-----	2.19

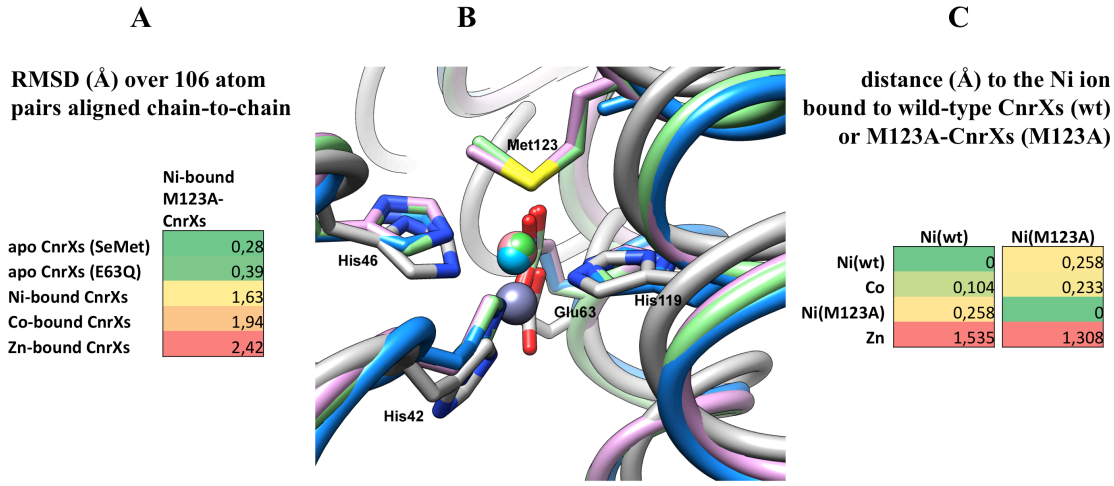

Fig. SI2. Binding of Ni(II) to M123A-CnrXs fail to promote the conformational change that was observed in wild-type CnrXs upon Ni(II) binding. *A*, Various metal-bound CnrXs dimers were superimposed. Reported is the RMSD measured between Ni-bound M123A-CnrXs (chain B) and the *apo*-form of a selenomethionine derivative of CnrXs (2y3g, chain C), the *apo*-form of E63Q-CnrXs (2y3h, chain C), Ni-bound CnrXs (2y39, chain A), Co-bound CnrXs (2y3b, chain A) or Zn-bound CnrXs (2y3d, chain B). *B*, Superimposition of the Cα of the residues common to all metal-binding sites highlights the similar location of Ni and Co ions as opposed to Zn(II). Note that the metal ions are almost aligned. Metal-chelating residues are named according to the three-letter code. Color code for proteins and metal ions: Ni-bound CnrXs, green; Ni-bound M123A-CnrXs, blue; Co-bound CnrXs, pink; Zn-bound CnrXs, grey. *C*, Distance between Ni(II) and other metal ions measured after metal-binding site superimposition. The Ni ion used as a reference was bound to either wild-type CnrXs (left) or M123A-CnrXs (right). Panel *B* was produced with the UCSF Chimera package (Resource for Biocomputing, Visualization, and Informatics at the University of California, San Francisco (supported by NIGMS P41-GM103311)).

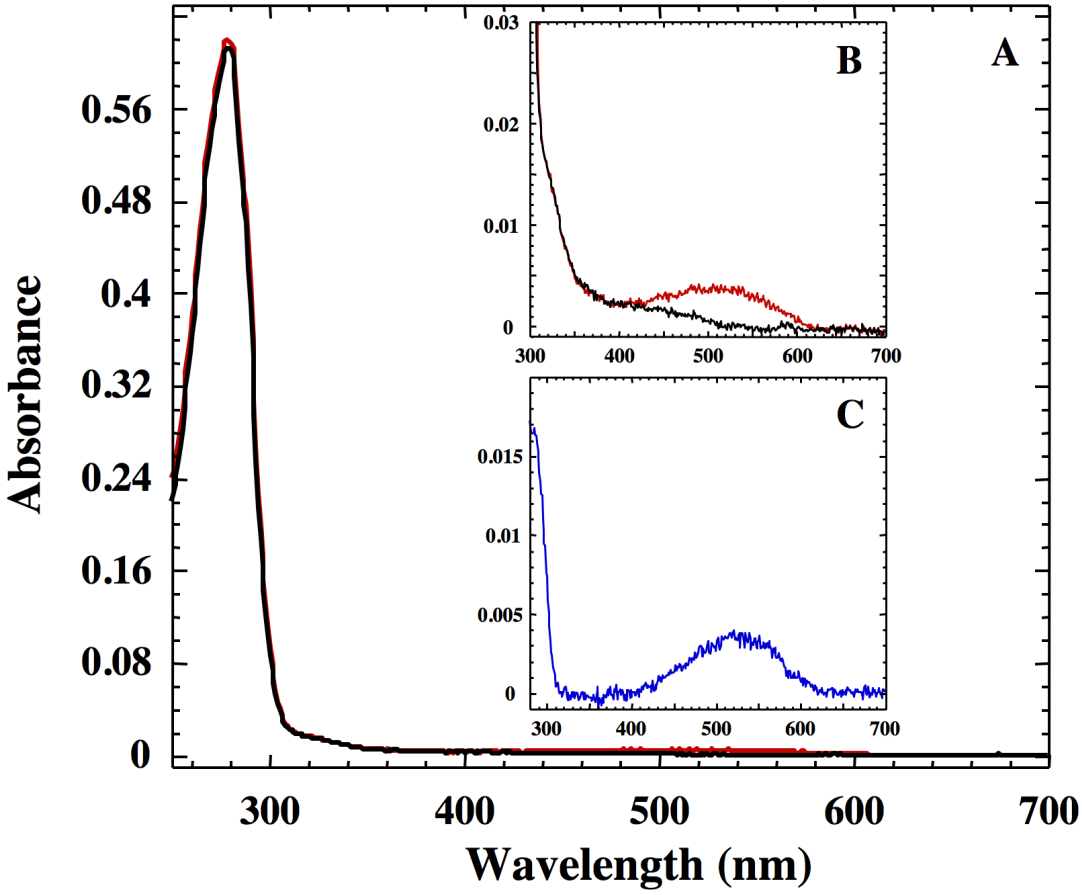

Fig. SI3. UV-visible spectroscopic characterization of Co-bound H32A-M123C-CnrXs. A: The spectrum of 36 µM *apo*-H32A-M123C-CnrXs was recorded (black spectrum). After addition of two Co-equiv, a new spectrum was recorded (red spectrum). Panel B is a magnification of the absorbance between 700 and 300 nm. The difference spectrum displayed in panel C was obtained by subtracting the black spectrum from the red one.

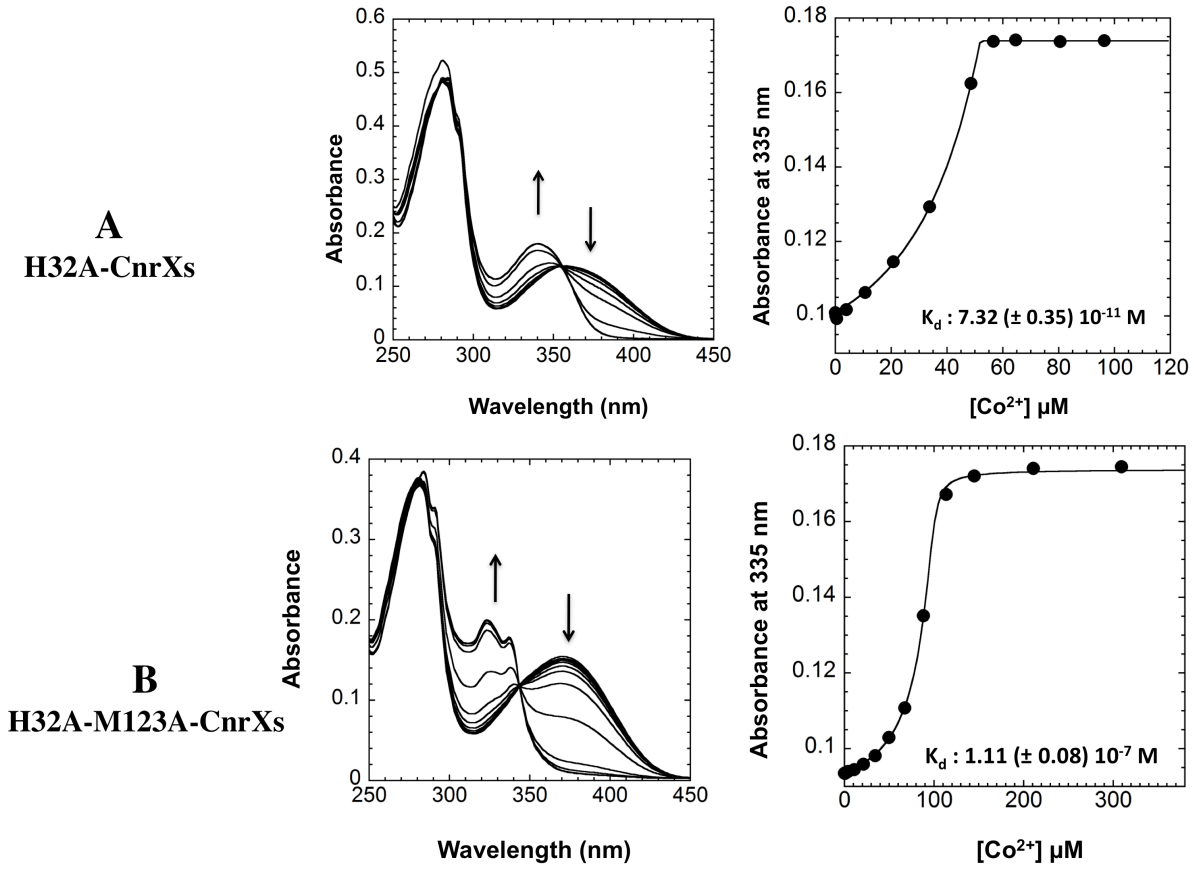

Fig. SI4. Spectrophotometric determination of the affinity of H32A-CnrXs and H32A-M123A-CnrXs for cobalt by competition with the chromogenic chelators fura-2 and mag-fura-2, respectively. Left panels : spectral evolution of (A) fura-2 (4.8 µM) in the presence of H32A-CnrXs (11.5 µM) and of (B) mag-fura-2 (5.2 µM) in the presence of H32A-M123A-CnrXs (47 µM), upon iterative additions of $CoCl_2$. Arrows indicate the spectral evolution. Right panels: absorption at 335 nm as a function of the Co(II) concentration. The solid lines represent the best fits associated with the indicated dissociation constants (Kd) and the standard errors. They were obtained with the program Dynafit using a single site model.

XAS: materials and methods, and selected references

For XAS experiments, 100 µL of 1-2 mM sample were transferred right after preparation to a PEEK home-made five-cell sample holder with a Kapton window, and flash-frozen in liquid nitrogen. X-ray absorption measurements were carried out at the European Synchrotron Radiation Facility (ESRF, Grenoble, France) which was operating with a ring current of 150 to 200 mA. Spectra were collected on the BM30B (FAME) beamline (1) using a Si(220) double crystal monochromator with dynamic sagital focusing. The photon flux was of the order of 10^{12} photons per second and the spot size was 300 µm horizontal x 50 µm vertical. The sample-holder was loaded in a helium cryostat with temperature set to 10K during data collection. All spectra were collected in fluorescence mode by measuring the Co-*K*α fluorescence with a 30-element solid-state Ge detector (Canberra). For each sample, four to six scans of 40 min each were averaged. Energy calibration was achieved by measuring a cobalt foil and assigning the first inflection point of the spectrum to 7709.0 eV. For the XANES analysis, pre-edge features were compared with those of Co(II) acetate tetrahydrate and Co(II)(2-methylimidazole)$_4$(BF4)$_2$ (2). EXAFS data analysis was performed using the IFEFFIT package (3). E_0 was defined at the half height of the absorption edge step. k^3-weighted EXAFS spectra were Fourier transformed over the k range 2.6-12.9 Å^{-1} using a Hanning window (α = 1.0). Fits were performed on the Fourier filtered spectra over the R range 0.9-4.0 Å. Theoretical amplitude and phase shift functions, including multiple scattering paths within the imidazole ring, were calculated with the *ab initio* code FEFF 6.0 using the structure of Co-bound CnrXs crystals determined by X-ray diffraction (4).

1. Proux, O., Nassif, V., Prat, A., Ulrich, O., Lahera, E., Biquard, X., Menthonnex, J.-J., and Hazemann, J.-L. (2006) Feedback system of a liquidnitrogen-cooled double-crystal monochromator: design andperformances. *J. Synchrotron Radiat.* **13**, 59-68.
2. Adrait, A., Jacquamet, L., Le Pape, L., Gonzalez de Peredo, A., Aberdam, D., Hazemann, J.-L., Latour, J.-M., and Michaud-Soret, I. (1999) Spectroscopic and saturation magnetization properties of the manganese- and cobalt-substituted Fur (ferric uptake regulation) protein from *Escherichia coli*. *Biochemistry* **39**, 6248-6260.
3. Ravel, B., and Newville, M. (2005) *ATHENA*, *ARTEMIS*, *HEPHAESTUS*: data analysis for X-ray absorption spectroscopy using *IFEFFIT*. J. Synchrotron Radiat. **12**, 537-541.
4. Trepreau, J., Girard, E., Maillard, A.P., de Rosny, E., Petit-Haertlein, I., Kahn, R., and Covès, J. (2001) Structural basis for metal sensing by CnrX. *J. Mol. Biol.* **408,** 408-766.

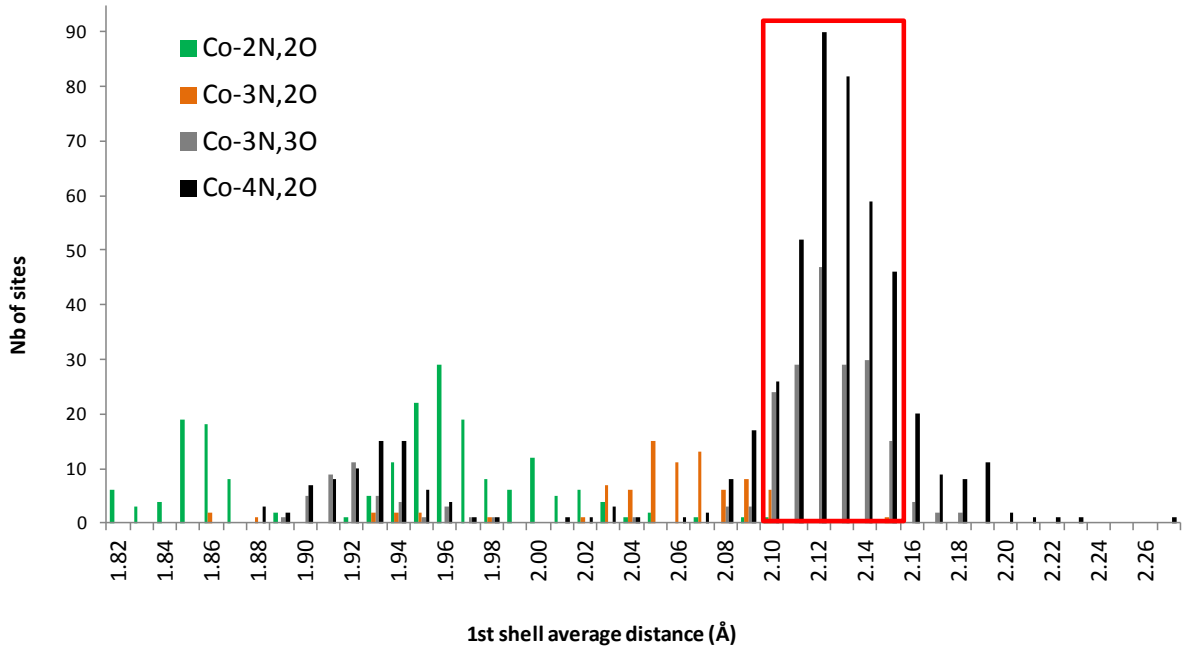

Fig. SI5. Averages of Co-O and Co-N first shell distances for small organic compounds from the CSD database, and range of distances found for two Co-bound H32A-M123A-CnrXs (red rectangle).

Table SI3: "Co-Met" data: computed spectroscopic data for the first 30 transitions used to simulate the UV-visible spectrum of Co-bound H32A-CnrXs. Transitions' numbers (#), excitation energies E (in a.u. and eV), and oscillator strengths f (in a.u.). Geometry of the molecular model constructed from PDB entry 2y3b. Conversion factor from eV to nm: nm = 1240/eV.

#	E/a.u.	E/eV	f
1	0.49231E-01	1.3396	0.18745E-03
2	0.51755E-01	1.4083	0.57645E-03
3	0.82272E-01	2.2387	0.22159E-02
4	0.86398E-01	2.3510	0.14665E-03
5	0.89709E-01	2.4411	0.37564E-02
6	0.90683E-01	2.4676	0.31170E-02
7	0.95272E-01	2.5925	0.49934E-03
8	0.10021	2.7270	0.24499E-02
9	0.10141	2.7596	0.90099E-03
10	0.10369	2.8215	0.57432E-03
11	0.10687	2.9081	0.25064E-03
12	0.11293	3.0729	0.83262E-03
13	0.11526	3.1364	0.26547E-02
14	0.12908	3.5124	0.67949E-02
15	0.13397	3.6454	0.54352E-02
16	0.13531	3.6821	0.43124E-01
17	0.13547	3.6864	0.12731E-01
18	0.14049	3.8229	0.42260E-02
19	0.14109	3.8392	0.21780E-02
20	0.14238	3.8743	0.39565E-02
21	0.14327	3.8986	0.28981E-02
22	0.14483	3.9410	0.47447E-03
23	0.14515	3.9496	0.13224E-02
24	0.14692	3.9978	0.53464E-03
25	0.14751	4.0141	0.15871E-02
26	0.14935	4.0641	0.56743E-02
27	0.14941	4.0656	0.20251E-03
28	0.14961	4.0710	0.26783E-02
29	0.14998	4.0812	0.34801E-02
30	0.15075	4.1022	0.97870E-02

The corresponding spectrum is represented in Fig. 8A of the main text.

Table SI4: "Co-Wat" data: computed spectroscopic data for the first 30 transitions used to simulate the UV-visible spectrum of Co-bound H32A-M123A-CnrXs. Transitions' numbers (#), excitation energies E (in a.u. and eV), and oscillator strengths f (in a.u.). Geometry of the molecular model constructed from PDB entry 2y3b: d(Co-O) = 2.2 Å). Conversion factor from eV to nm: nm = 1240/eV.

#	E/a.u.	E/eV	f
1	0.53013E-01	1.4425	0.12694E-03
2	0.54041E-01	1.4705	0.33384E-03
3	0.81327E-01	2.2130	0.39814E-02
4	0.82161E-01	2.2357	0.19332E-02
5	0.90096E-01	2.4516	0.30067E-03
6	0.93641E-01	2.5481	0.39983E-03
7	0.96173E-01	2.6170	0.23565E-02
8	0.98232E-01	2.6730	0.36443E-03
9	0.10082	2.7435	0.36885E-03
10	0.10857	2.9544	0.14798E-03
11	0.11191	3.0452	0.24197E-02
12	0.11947	3.2509	0.10730E-02
13	0.12167	3.3108	0.24732E-03
14	0.12280	3.3415	0.11253E-03
15	0.13174	3.5849	0.15450E-01
16	0.13661	3.7173	0.67141E-03
17	0.13692	3.7258	0.25900E-03
18	0.13805	3.7566	0.11174E-01
19	0.14059	3.8256	0.24047E-03
20	0.14174	3.8569	0.42869E-04
21	0.14232	3.8728	0.10507E-02
22	0.14653	3.9872	0.12675E-01
23	0.14833	4.0362	0.57738E-02
24	0.14873	4.0473	0.16616E-02
25	0.15395	4.1891	0.71354E-02
26	0.15571	4.2371	0.11039E-02
27	0.15618	4.2499	0.15142E-03
28	0.15708	4.2743	0.47238E-03
29	0.15722	4.2783	0.37308E-02
30	0.15838	4.3098	0.17419E-02

The corresponding spectrum is represented in Fig. 8B of the main text.